JOURNAL OF COLLOID AND INTERFACE SCIENCE **203,** 335–344 (1998)
ARTICLE NO. CS985499

Stabilizing the Advancing Front of Thermally Driven Climbing Films

Dawn E. Kataoka and Sandra M. Troian[1]

Department of Chemical Engineering, Princeton University, Princeton, New Jersey 08544-5263

Received September 8, 1997; accepted February 26, 1998

As known from thermodynamic principles, the surface tension of a liquid decreases with increasing temperature. This property can be used to force a liquid film to climb a vertical substrate whose lower end is held warmer than the top. The vertical gradient in surface tension generates a surface shear stress that causes the liquid film to spread upward spontaneously in the direction of higher surface tension. Experimental investigations have shown that the application of a large temperature gradient produces a thin climbing film whose leading edge develops a pronounced capillary rim which breaks up into vertical rivulets. In contrast, smaller temperature gradients produce thicker films whose profiles decrease monotonically toward the substrate with no evidence of a rim or subsequent film breakup. We have previously shown within linear stability analysis that a climbing film can undergo a fingering instability at the leading edge when the film is sufficiently thin or the shear stress sufficiently large for gravitational effects to be negligible. In this work we show that thicker films which experience significant drainage cannot form a capillary rim and spread in stable fashion. Gravitational drainage helps promote a straight advancing front and complete surface coverage. Our numerical predictions for the entire shape and stability of the climbing film are in good agreement with extensive experiments published years ago by Ludviksson and Lightfoot (*AIChE J.* 17, 1166 (1971)). We propose that the presence of a counterflow which eliminates the capillary rim can provide a simple and general technique for stabilizing thermally driven films in other geometries.

Key Words: **drainage; thermally driven spreading; coating films; Marangoni forces.**

INTRODUCTION

Thermodynamic considerations of the surface entropy at an air–liquid interface at finite temperature dictate that the surface tension of a liquid is a decreasing function of temperature. This property can be used to generate climbing films which coat surfaces in vertical geometries. Subjecting a vertical substrate to a temperature gradient whose lower end is warmer than the top will produce an upwardly directed surface tension gradient in an adjacent liquid film. The surface tension gradient, which depends on the particular temperature distribution along the substrate, creates a surface shear stress that forces the liquid film to climb above the position of the equilibrium meniscus. Concentration variations at an air–liquid interface, which are more difficult to control, can produce a similar shear stress which causes a liquid coating to spread upward against gravity. Such ''supermeniscus'' films have been shown to be important in the operation of gas diffusion electrodes in which the oxidation reaction occurs almost exclusively in the region above the normal meniscus position (1). Enhanced spreading behavior has also been observed in boundary lubrication problems in which the evaporation of volatile impurities in the spreading films establishes a spontaneous concentration gradient (2). Flows created by gradients in surface tension, whether induced by temperature or concentration variations, are commonly called thermocapillary or Marangoni-driven flows. These types of flows, which become dominant in situations where the surface-to-volume ratio of the liquid film is large, are receiving increased attention as technological advances encourage the production of smaller and lighter componentry.

Although temperature or concentration gradients can therefore be used very effectively to guide a spreading film to coat a substrate, the coating process will be unsuccessful if the liquid spreads nonuniformly and suffers any instability at the leading edge. Several groups have shown that thermally driven films are subject to a fingering instability at the advancing front. In coating experiments of horizontal (3) or vertical substrates (4, 5), thermally driven films were observed to develop a pronounced capillary rim at the leading edge. This rim separated rather quickly into numerous thin, parallel rivulets which remained a fixed distance apart and never coalesced. Earlier experiments by Ludviksson and Lightfoot (LL), however, showed that uniform stable coatings are easily achievable with thermally forced films (6). Reconstruction of the film thickness profiles from interferometry indicated that the coating films thinned monotonically toward the substrate with no evidence of a capillary rim at the leading edge of the spreading film. In both the stable and unstable situations, the fluids that were used were known to be completely wetting against the substrate material, so the difference in behavior cannot be attributed to

[1] To whom correspondence should be addressed.

0021-9797/98 $25.00

wettability problems. A comparison of the relevant parameters from all the available experiments (7) reveals, however, the critical role of gravity in stabilizing the advance of a spreading film. While the experiments employing larger thermal gradients produced thinner spreading films for which gravitational drainage or hydrostatic effects can be ignored, the ones employing smaller thermal gradients produced thicker films which, in vertical geometry, were strongly modified by drainage.

In previous work, we investigated the spreading behavior and linear stability of thermally driven films for which the effects of gravity were negligible (7, 8). The shape of the spreading film, the speed of advance, and the value of the most unstable wavelength agreed very well with all available experimental data for unstable films. This analysis revealed a strong correlation between the formation of a capillary rim at the leading edge and a subsequent fingering instability at this location. The stable climbing films produced by LL were outside the parameter range of our previous calculations. For the thicker films produced by LL, the downward flux due to gravitational drainage is comparable to the upward flux due to Marangoni forces. In this paper we extend our previous analysis by including a counter-flow term due to gravitational drainage. We show how the presence of this additional term eliminates the capillary rim to produce a flow which is linearly stable to perturbations of all wavenumbers. Detailed comparison between the numerical profiles and the interferometric measurements by LL for constant shear stress reveals very good agreement despite the inherent experimental uncertainty in the overall film thickness.

PROBLEM FORMULATION

For simplicity we consider the case of a Newtonian liquid film, of density ρ and viscosity η, climbing a vertical substrate bearing a constant temperature gradient. With the warmer region located at the lower end, the film experiences a constant upward surface shear stress, τ, which counteracts the downward acceleration of gravity, g. In the lubrication approximation, the interfacial curvature provides a pressure gradient at the air–liquid interface and throughout the film. Within the ''inner region'' close to the advancing edge, where Marangoni, gravity, viscous, and capillary forces contribute, the governing lubrication equations become

$$\eta \frac{\partial^2 u}{\partial z^2} = \frac{\partial p}{\partial x} + \rho g, \qquad [1]$$

$$\eta \frac{\partial^2 v}{\partial z^2} = \frac{\partial p}{\partial y}, \qquad [2]$$

$$\frac{\partial p}{\partial z} = 0, \qquad [3]$$

where x represents the direction of flow, y the direction transverse to the flow, and z the direction perpendicular to the substrate as shown in Fig. 1. The velocity components u and v represent flow in the x and y directions, and p denotes the local pressure in the film. Within the thin film approximation, the capillary pressure is approximated by $\Delta p = -\gamma \nabla^2 h$ for small slopes, where $h(x, y, t)$ locates the position of the air–liquid interface and γ the local surface tension. In addition, the term coupling the interfacial curvature, $\nabla^2 h$, to the gradient in surface tension, $\nabla \gamma$, can be ignored in the inner region (7). In what follows we consider variations in surface tension that are significantly larger than variations in the fluid density or viscosity which are therefore held constant. Also, for liquid films whose thickness is in the micron range, the Biot number $\mathrm{Bi} = hd/k \ll 1$, where h is the heat transfer coefficient of the air phase (of order 10^4 erg/cm^2 s °C), d the characteristic film thickness (of order 10^{-4} cm), and k the thermal conductivity of the liquid film (of order 10^4 erg/cm s °C). The ratio of the conductive resistance to the convective resistance is very small, and the local temperature of the liquid film can therefore be approximated by the local temperature of the substrate. The lubrication equations are solved subject to the boundary conditions of no-slip at the solid surface,

$$u, v|_{z=0} = 0, \qquad [4]$$

and constant shear stress, $\tau = (d\gamma/dT)(dT/dx)$, at the air–liquid interface,

$$\eta \left.\frac{\partial u}{\partial z}\right|_{z=h} = \tau. \qquad [5]$$

Since for many liquids $d\gamma/dT$ is constant over a reasonable temperature range, a constant shear stress simply requires the application of a linear temperature profile. The resulting height-averaged velocities are

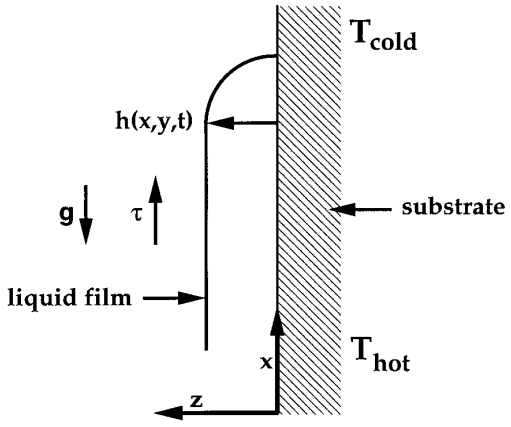

FIG. 1. Schematic of liquid film climbing a vertical substrate.

$$U(x, y) = \frac{\tau h}{2\eta} + \frac{\gamma h^2}{3\eta}\frac{\partial}{\partial x}(\nabla^2 h) - \frac{\rho g h^2}{3\eta}, \quad [6]$$

$$V(x, y) = \frac{\gamma h^2}{3\eta}\frac{\partial}{\partial y}(\nabla^2 h). \quad [7]$$

The film thickness profiles can be determined by substituting the velocities into the kinematic boundary condition at the air–liquid surface which yields the interface equation,

$$\frac{\partial h}{\partial t} + \frac{\partial}{\partial x}(hU) + \frac{\partial}{\partial y}(hV) = 0. \quad [8]$$

We reduce this equation to nondimensional form by appropriate rescaling. The characteristic film thickness is set by the film thickness far from the leading edge,

$$h_c = \alpha\frac{\tau}{\rho g}, \quad [9]$$

where α is a proportionality constant corresponding to the relative strength between the drainage and thermocapillary forces. The coordinates x and y are rescaled by the length of the inner region, l, over which capillary forces are operable (9–12):

$$l = h_c(3\mathrm{Ca})^{-1/3}, \quad [10]$$

where the capillary number is defined by $\mathrm{Ca} = \eta U_c/\gamma$. The characteristic spreading velocity, U_c, is given by

$$U_c = \frac{\tau h_c}{2\eta} - \frac{\rho g h_c^2}{3\eta} = \frac{\tau^2}{\rho g \eta}\frac{\alpha}{2}\left(1 - \frac{2\alpha}{3}\right). \quad [11]$$

The value $\alpha = \frac{3}{2}$ corresponds to no net liquid flux, while the value $\alpha = \frac{3}{4}$ represents the maximum upward flux. We restrict our attention to climbing films for which $\alpha < \frac{3}{2}$. This choice of scalings yield the following dimensionless variables:

$$\xi = -\frac{x}{l}, \quad \zeta = \frac{y}{l}, \quad \bar{h} = \frac{h}{h_c},$$

$$\bar{t} = \frac{t}{l/U_c}, \quad \bar{U} = \frac{U}{U_c}, \quad \bar{V} = \frac{V}{U_c}.$$

The ξ coordinate is reversed in sign so that upward spreading tends toward $\xi \to -\infty$. We solve the dimensionless interface equation by requiring that the film achieve a thickness, h_c, behind the leading edge and thickness $bh_c (b \ll 1)$ in front of the leading edge. This prewetted layer represents a precursor film. Previous studies have discussed the usefulness of employing a precursor film in theoretical or numerical studies in order to alleviate the stress singularity arising from the application of the no-slip condition at a moving contact line (7, 12–15). Ludviksson and Lightfoot, however, noted the very real presence of a precursor film in their experiments, making this boundary condition a realistic choice for our numerical solutions.

Substituting the rescaled form of Eqs. [6] and [7] into the dimensionless form of Eq. [8] yields the governing equation for the film thickness:

$$h_t - \left[\frac{3}{3-2\alpha}h^2 - \frac{2\alpha}{3-2\alpha}h^3 - h^3(\nabla^2 h)_\xi\right]_\xi + [h^3(\nabla^2 h)_\zeta]_\zeta = 0, \quad [12]$$

where $\nabla^2 = \partial_{\xi\xi} + \partial_{\zeta\zeta}$. The overbars have been dropped for convenience. In rescaled form, the appropriate boundary conditions for h become

$$h \to 1 \quad \text{as} \quad \xi \to \infty, \quad [13]$$

$$h \to b \quad \text{as} \quad \xi \to -\infty, \quad [14]$$

where b is the dimensionless precursor film thickness.

RESULTS

Base Flow

We seek traveling wave solutions of constant speed c for both the base and disturbed flow:

$$h(\xi, \zeta, t) = h_0(\xi + ct) + h_1(\xi + ct, \zeta, t), \quad [15]$$

where h_0 represents the base flow solution and h_1 represents an infinitesimal two-dimensional disturbance. In the experiments of LL, which were designed to provide a constant liquid flux, the leading edge of the spreading film was observed to travel at constant speed in accordance with the solutions sought. Substitution of this form into Eq. [12] yields the governing fourth-order equation for the base state:

$$ch_{0\xi} - \frac{3}{3-2\alpha}(h_0^2)_\xi + \frac{2\alpha}{3-2\alpha}(h_0^3)_\xi + (h_0^3 h_{0\xi\xi\xi})_\xi = 0. \quad [16]$$

Integrating Eq. [16] once, subject to the boundary conditions that the film profile match onto a uniformly flat film at either extreme ($\xi = \pm\infty$), yields the equation

$$h_{0\xi\xi\xi} = \frac{3}{(3-2\alpha)h_0} - \frac{2\alpha}{3-2\alpha} - \frac{3(1+b) - 2\alpha(1+b+b^2)}{(3-2\alpha)h_0^2} + \frac{(3-2\alpha)b - 2\alpha b^2}{(3-2\alpha)h_0^3}, \quad [17]$$

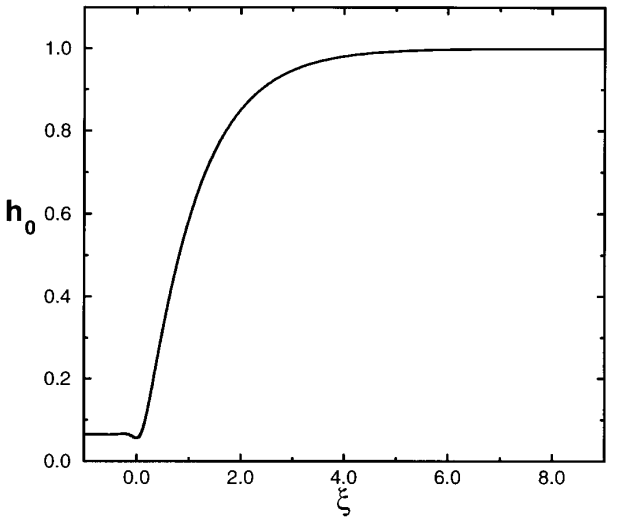

FIG. 2. Numerical solution of dimensionless base flow profile, $h_0(\xi)$, for $\alpha = 1$.

where the dimensionless wave speed is determined to be $c = [3(1 + b) - 2\alpha(1 + b + b^2)]/(3 - 2\alpha)$. Equation [17] is converted into three first-order equations for which the resulting initial value problem is solved in similar fashion to other free surface problems involving capillary flows (11, 15, 16). Linearizing about the boundary condition $h_0 \to 1$ as $\xi \to +\infty$ provides the starting values for the integration,

$$h_0 \to 1 - a\exp(-c^{1/3}\xi) \quad \text{as} \quad \xi \to \infty, \qquad [18]$$

where a is a small parameter. In practice, we retain higher order terms to provide additional refinement for the initial value.

Since Eq. [17] is translationally invariant, different choices in the starting position ξ merely shift the position of the overall film profile in the spreading direction. For a given starting position and choice of parameter a we obtained profiles that satisfied Eq. [17] and the required boundary conditions by making small adjustments in the thickness of the precursor layer, b. Fixing the value of b and floating the parameter a produced the same solution. Shown in Fig. 2 is the numerical solution for $\alpha = 1$. The film thickness decreases smoothly and monotonically from the thicker portion of the film toward the precursor layer with no evidence of a capillary rim at the leading edge. Smaller values of α are found to produce film profiles with larger values of b.

Previous calculations in the literature for thermocapillary driven films have included a disjoining pressure term in the equation governing the film thickness (16). This term is operable only in the thinnest portions of the liquid film. To mimic the influence of van der Waals forces for a nonpolar wetting film on a high energy surface, we also included on the right hand side of Eq. [17] a term A_0/h_0^4, where $A_0 = A_{\text{Ham}}l^2/2\pi\gamma h_c^4$ and A_{Ham} denotes the Hamaker constant. The numerical profiles with or without the inclusion of the van der Waals term are virtually identical, with the exception of tiny differences in the precursor layer thickness. Since the film thickness and lateral extent of the capillary region are still large compared to the length scale over which van der Waals forces can contribute, their inclusion does not change the overall film shape leading away from the precursor film. We therefore safely neglected this term in the stability calculations described next.

Linear Stability Analysis

We seek linearized disturbance solutions to the flow, h_1, which are periodic in the transverse direction and travel at constant speed:

$$h_1(\xi + ct, \zeta, t) = G(\xi + ct)\exp(iq\zeta + \beta t). \qquad [19]$$

The parameter q represents the dimensionless wavenumber and β represents the disturbance growth rate. Linearizing Eq. [12] yields the eigenvalue equation for the disturbance function G,

$$\beta G + \frac{3(1 + b) - 2\alpha(1 + b + b^2)}{(3 - 2\alpha)} G_\xi - \frac{\partial}{\partial\xi}\left[\frac{6}{3 - 2\alpha} h_0 G - \frac{6\alpha}{3 - 2\alpha} h_0^2 G - 3h_0^2 h_{0\xi\xi\xi} G - h_0^3(G_{\xi\xi\xi} - q^2 G_\xi)\right] + h_0^3(q^4 G - q^2 G_{\xi\xi}) = 0, \qquad [20]$$

which must satisfy the boundary conditions

$$G, G_\xi \to 0 \quad \text{as} \quad \xi \to \pm\infty. \qquad [21]$$

Equation [20] was discretized by using a central difference scheme on the same nonuniform mesh used to solve the base flow. The eigenvalues and eigenfunctions were obtained by using RGG, a standard QR algorithm in the EISPACK library (17). The dispersion curve, $\beta(q)$, for the case $\alpha = 1$ is shown in Fig. 3. The flow is linearly stable since $\beta(q)$ is everywhere negative for $q > 0$. As will be discussed later, all values of α derived from the experiments of LL (wherein $0.0.862 \le \alpha \le 1.16$) yielded linearly stable flows, in accordance with their findings. The shape of the eigenfunction, G, for the parameter value $\alpha = 1$ is shown in Fig. 4 for different choices of wavenumber. While the shape of the eigenfunction right at the advancing front seems unaffected by the wavenumber of the disturbance, larger wavenumbers enhance the function behind the leading edge. Smaller values of q produce slightly faster decay to the uniform flat film as $\xi \to \infty$. The region of rapid variation in

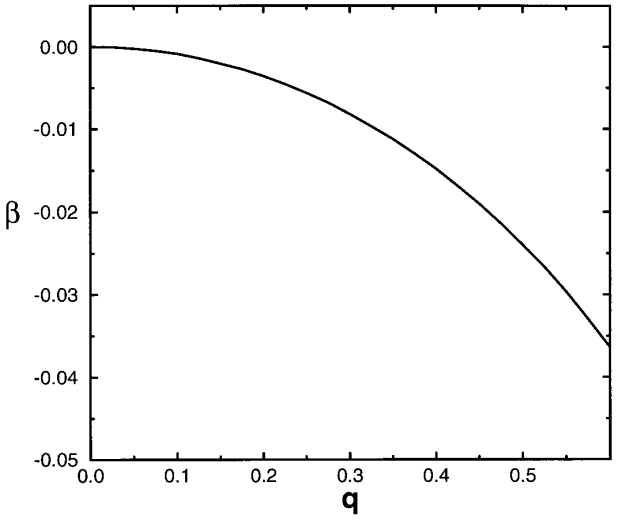

FIG. 3. Dispersion curve, $\beta(q)$, associated with eigenfunction $G(\xi)$ for $\alpha = 1$.

G corresponds directly to the precipitous portion of the base flow, h_0, where the flat film decreases sharply to meet the precursor layer. This disturbance analysis clearly demonstrates that drainage stabilizes the flow against any fingering instability at the spreading front. We report in the next section results of a simple energy analysis which compares the relative strengths of all the forces affecting the climbing film.

Energy Analysis

The following energy breakdown (12) describes how each term in the disturbance equation, Eq. [20], generates or deletes energy from the flow. Negative contributions promote stability and vice versa. One can associate a ''mechanical energy'' with the disturbance by defining the inner product:

$$E = \frac{1}{2}\langle h_1, h_1\rangle = \frac{1}{2}\int_{-\infty}^{+\infty} (h_1)^2 d\xi. \qquad [22]$$

To relate the rate of energy production to the eigenfunction, G, the disturbance equation [20] is first recast in operator form,

$$h_{1t} + L_{h_0}[h_1] = 0, \qquad [23]$$

where the linear operator, L_{h_0}, which depends explicitly on the base flow solution, h_0, includes all the terms with spatial derivatives in Eq. [20]. Substituting Eq. [23] into the expression for the rate of energy production, $dE/dt = \langle h_1, \dot{h}_1\rangle$, yields

$$\frac{dE}{dt} = \beta\langle G, G\rangle = -\langle G, L_{h_0}[G]\rangle. \qquad [24]$$

The growth rate, β, defines the normalized, dimensionless rate of energy production, $\dot{E}_{\text{tot}}$:

$$\beta = \dot{E}_{\text{tot}} = -\frac{\langle G, L_{h_0}[G]\rangle}{\langle G, G\rangle}. \qquad [25]$$

The physical origin of the eight terms contained in L_{h_0} is listed in Table 1. To associate an energy production rate with each of these eight terms, we define the quantity

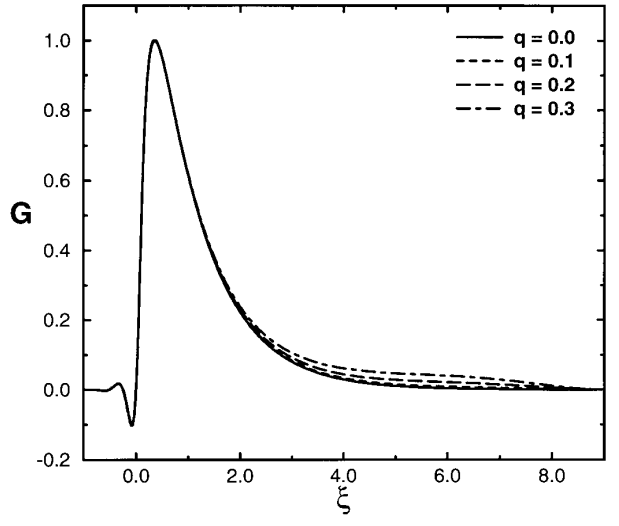

FIG. 4. Eigenfunction $G(\xi)$ corresponding to different values of q for branch shown in Fig. 3.

TABLE 1
Terms Contributing to Energy Production Rate

Term	Expression	Physical mechanism
1	cG_ξ	Streamwise convection from moving reference frame
2	$\frac{\partial}{\partial\xi}(h_0^3 G_{\xi\xi\xi})$	Streamwise capillary flow induced by $G_{\xi\xi\xi}$
3	$-\frac{\partial}{\partial\xi}(q^2 h_0^3 G_\xi)$	Streamwise capillary flow induced by G_ξ
4a	$-\frac{\partial}{\partial\xi}\left(\frac{6}{3-2\alpha} h_0 G\right)$	Streamwise Marangoni flow induced by G
4b	$\frac{\partial}{\partial\xi}\left(\frac{6\alpha}{3-2\alpha} h_0^2 G\right)$	Streamwise drainage induced by G
5	$\frac{\partial}{\partial\xi}(3h_0^2 h_{0\xi\xi\xi} G)$	Streamwise capillary flow induced by G
6	$-q^2 h_0^3 G_{\xi\xi}$	Transverse capillary flow induced by $G_{\xi\xi}$
7	$q^4 h_0^3 G$	Transverse capillary flow induced by $h_{1\zeta\zeta\zeta\zeta}$

$$\dot{E}_n = -\frac{\langle G, L_{h_0,n}[G]\rangle}{\langle G, G\rangle}, \qquad [26]$$

where n represents the number assigned to each term in Table 1. For all wavenumbers, the eight contributions to the energy sum to the value $\beta(q)$, as was checked numerically. In Fig. 5a is plotted the strength of each term as a function of the disturbance wavenumber for the case $\alpha = 1$.

The most dominant terms affecting the stability characteristics of the climbing film in the streamwise direction are the destabilizing Marangoni shear stress and the stabilizing drainage force represented by terms 4a and 4b, respectively. Since term 4b scales with h_0^2 while term 4a scales linearly with h_0, the former term is slightly larger in magnitude for all q because $h_0 \leq 1$. A magnified view of the contributions which only slightly affect film stability is shown in Fig. 5b. These include terms 1, 3, 6, and 7. Term 1 is completely neutral (i.e. $\dot{E}_1(q) = 0$) since it represents the convective flow contribution upon changing reference frame to a steadily moving traveling wave. Terms 3, 6, and 7 are the convective terms created by capillary flow in either the streamwise or transverse directions. The latter two terms are often associated with the Rayleigh-like distribution of fluid that occurs in a cylindrical column of liquid as described previously (7, 12). Each of these smaller terms depends at most on the second derivative of the disturbance function, $G_{\xi\xi}$, or the first derivative of the base flow, $h_{0\xi}$. The other two capillary terms, 2 and 5, which induce flow in the streamwise direction are significantly larger (and stabilizing) since they depend on higher derivatives of G and h_0, which can be extremely large in the part of the advancing front meeting the precursor layer. As evident from Fig. 5a, drainage and streamwise capillary flow due to the strong curvature in h_0 and G overcome the destabilizing effects of Marangoni shearing forces. Even though the base flow shows no evidence of a capillary rim which rises above the flat portion of the film, as we observed in unstable flow, the functions h_0 and G still display significant curvature. The higher order derivatives of these functions strongly contribute either positive or negative sums to the rate of energy production. The rich spatial structure displayed by the eigenfunctions signal the strong response produced by infinitesimal disturbances of any wavenumber. Despite the sharpness of the eigenfunctions at the leading edge, the liquid film is stabilized by the presence of the gravity counterflow.

DISCUSSION AND COMPARISON WITH EXPERIMENT

As briefly described in the Introduction, climbing films subject to stronger shear stresses produce thinner advancing films which destabilize in the manner predicted by our previous calculations. For example, Cazabat and coworkers (4, 5) reported a well-formed fingering instability at the leading edge of a climbing film which developed within minutes of applying a vertical temperature gradient. In these experiments, a silicone oil film subject to stresses of approximately 0.5 dyn/cm^2 and higher was made to coat a silicon wafer. In contrast, earlier experiments by LL (6) using squalane oil spreading on a silver substrate with surface stresses of the order of 0.2 dyn/cm^2 or less seemed to produce stable spreading films with a straight-edged moving front. Using interferometry, they reconstructed the film thickness profiles and showed that the film shape decreased monotonically toward the substrate with no evidence of a capillary rim at the advancing front.

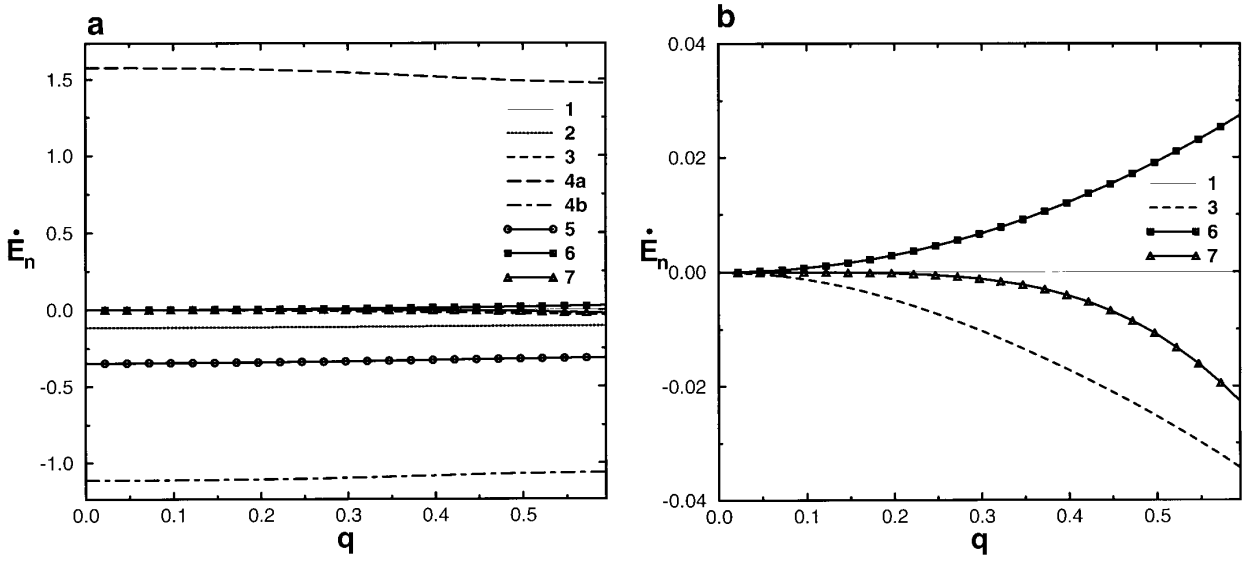

FIG. 5. (a) Contribution of each term in Table 1 to overall energy production rate for $\alpha = 1$. (b) Magnified view of (a) near the axis $\dot{E}_n = 0$.

They noted in passing the presence of a discolored and darker region ahead of the visible front which they attributed to a precursor film. This film may have been created during the preparation stage when the silver substrate was prewetted by dipping it into the squalane reservoir. It may also have developed as a diffusing film from the leading edge of the spreading squalane during the very long experimental runs which lasted from 10 to 24 h.

In order to generate the numerical profiles to compare with experiment, we used Eq. [9] and the experimental values from LL to determine the value of α corresponding to each of the five experimental runs reported by LL. The experimental values for h_c, τ, and ρ are required as input. As noted by LL, the thickest part of the film, h_c, is only known to within 0.0938 μm, since the position of the first-order fringe emanating from the precursor layer can only be estimated approximately. In addition, the data points corresponding to the thickest parts of the spreading film are the most unreliable since the flattest portion produces very broad fringes whose position is difficult to measure. Nonetheless, we used the values quoted by LL for this limiting film thickness to reproduce the appropriate curves in dimensional form. The liquid density of the squalane was calculated at the average temperature of the substrate for each of five experiments according to the curve for $\rho(T)$ provided by LL. All relevant parameters used to generate the numerical curves are listed in Table 2. Figure 6 is a comparison of the numerical solutions for all five experiments. The error bars shown on the curve $\tau = 0.133$ dyn/cm^2 correspond in magnitude to 2×0.0938 μm. The actual experimental profiles lie somewhere within this error range. The theoretical curves in Fig. 6 were first generated by choosing the value of α corresponding to the value of h_c reported by LL. We then shifted the profiles slightly in the vertical direction (recall that the horizontal shift is arbitrary) in order for the curves to best fit the experimental data. For the case $\tau = 0.147$ dyn/cm^2, the last data point lies well outside the theoretical prediction. It is interesting that LL specifically mentioned the difficulty they had in determining the highest order fringe for this particular experiment. The agreement between the experimental and numerical profiles for the film shape is fairly good except for the lowest shear stress, $\tau = 0.086$ dyn/cm^2. Unlike the theoretical prediction, this experimental profile displays no curvature at the leading edge and is unlike any of the other profiles measured by LL. Since no experimental explanation was provided for this suspect behavior, it is not of concern that the theoretical prediction fails to reproduce this unusual shape. Perhaps another mechanism like surface diffusion, which is not included in the model, can account for this behavior.

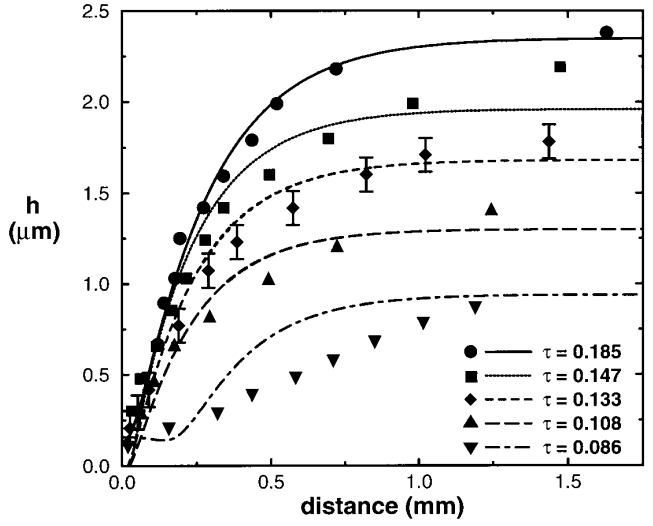

FIG. 6. Comparison of numerical and experimental film thickness profiles. Values of τ are in units of dyn/cm^2. Filled symbols represent experimental data (6). Solid and dashed lines represent theoretical solutions.

The agreement shown in Fig. 6 is surprisingly good given the inherent measurement error in several of the important parameters required by the theory. The agreement for the larger values of τ seems slightly better. This can be understood by noting some details about the temperature measurements. Although LL reported that the applied temperature gradients were linear to within about 5%, their measurements indicated that the temperature profiles along the vertical substrate exhibited some nonlinearity close to the warmer region where they recorded a higher temperature gradient. The nonlinearity was more pronounced for smaller temperature differences between the warm and cool ends. Besides this error, the accuracy of the thermistor reading along the substrate becomes less reliable with smaller temperature gradients. For example, a typical 125 μm thermistor is at best accurate to ± 0.25°C. This uncertainty can yield errors as large as 25% for a temperature difference of 2°C, which corresponds to the smallest gradient used by LL. Another source of error stems from the inferred values of τ. LL stated that their values of $d\gamma/dT$ were only known within

TABLE 2
Results for Vertically Spreading Films Examined by Ludviksson and Lightfoot (6)[a]

h_{exp} (μm)	τ (dyne/cm^2)	ρ (g/cm^3)	α	$U_{tw}(h_c)$ (μm/s)	U_{exp} (μm/s)
0.94	0.086	0.805	0.862	0.0633	0.0531
1.40	0.108	0.816	1.04	0.0680	0.0714
1.78	0.133	0.798	1.05	0.138	0.139
2.16	0.147	0.806	1.16	0.132	0.178
2.35	0.185	0.803	1.00	0.289	0.249

[a] Values for α are calculated using Eq. [9]. The dimensional traveling wave speed U_{tw} is given by U_c (Eq. [11]) multiplied by the dimensionless traveling wave speed c.

5%. This estimate, coupled with a 5% or more error in the determination of the temperature gradient, dT/dx, can produce values of τ which are in error by at least 7%. It is clear from our numerical work that even better agreement can be achieved by accounting for these errors in the input values for the film shape.

Besides the shape of the spreading film, one can also compare the speed of the traveling wave solution with the measured speed of the climbing films, U_{exp}, for different values of the shear stress. In Fig. 9 of Ref. (6) the climbing speed of the spreading squalane films was indeed shown to remain constant after the first 4–6 h of spreading, which satisfies the steady state conditions of the model. All experimental measurements were taken after any transient behavior had died away. The model predicts a (dimensional) traveling wave speed,

$$U_{tw} = cU_c = \{[3(1 + b) - 2\alpha(1 + b + b^2)]/[3 - 2\alpha]\}(\tau h_c/2\eta - \rho g h_c^2/3\eta). \quad [27]$$

The comparison for the climbing speed is shown in Table 2. Agreement is quite good except for the case $\tau = 0.147$ dyn/cm^2. This discrepancy can probably be traced once again to the difficulty LL described in measuring the position of the last fringe in the thick part of the film used to determine h_{exp} and therefore h_c.

There is at least one other theoretical study in the literature by Teletzke *et al.* (16) describing the shape of thermally driven climbing films. In this work the governing third order equation for h_0 was also converted into an initial value problem and solved in a manner similar to that described above. Although the numerical profiles were in qualitative agreement with those measured by LL, quantitative comparison revealed that the extent of the capillary region over which the film shape bends to meet the precursor layer was only one-third as broad as indicated by the experimental profiles. We find that their discrepancy with experiment is at least partly due to algebraic errors in determining the correct linearized form of $h(\xi)$ required to initiate the integration scheme. In addition, when nondimensionalizing the equations, Teletzke *et al.* scaled both the film thickness and the extent by the same and rather sizable length scale, $(\gamma/\rho g)^{1/2}$. Although this may be a reasonable scale with which to non-dimensionalize the extent of the so called ''inner region'' where capillary forces compete with the other relevant forces, it seems an inappropriate scale for the film thickness, whose scale is set by the competition between Marangoni and drainage forces. The capillary length is typically of order millimeters while the film thicknesses in the experiments of LL were typically in the micron range. We instead chose different scalings for the film thickness and the ''inner region'' consistent with the lubrication approximation. Whether the previous disagreement noted by Teletzke *et al.* was due to algebraic errors or numerical problems associated with the choice of scaling parameters, we find that our scaling choice captures very well the extent and shape of the curved region near the advancing front. We have initiated an experimental program to collect data over a wider parameter range in order to test and further improve the model being used.

We have compared the shape of the climbing films, h_0, and the disturbance eigenfunctions, G, for both stable and unstable flows. In our previous work, it was shown explicitly that a capillary rim, whose height rises above the flat part of the spreading film, is required for instability. The disturbance function displayed a strong peak localized in the forward portion of the capillary rim. As the thickness of the precursor was increased to values approaching the original film thickness, the capillary rim vanished and the spreading process was stabilized against fingering instability at the leading edge. In this present work, we have shown that gravitational drainage depletes the contents of the capillary rim and produces a smoothly decreasing film profile with no evidence of a ''bump'' at the leading edge. The spreading is perfectly stable and advances over the solid substrate with a straight-edged front. One may wonder whether the instability is caused simply by the amplitude of the capillary rim or whether it is caused by the sizable curvature of the film profile near the leading edge. As shown in Figs. 2 and 4, however, even the stable fronts exhibit strong curvature at the leading edge. A careful comparison between the eigenfunctions shown in this study and those previously obtained by us for the unstable flow reveals practically the same shape at the leading edge. The differences become apparent behind the large peak where the disturbance must die away to meet the undisturbed film thickness. The disturbance function in Fig. 4 decays smoothly to zero as ξ increases, while the disturbance function for unstable flow (7) displays one oscillation after the peak is traversed. We believe it is this oscillation in the curve that leads to instability. This suggests that it is not so much the curvature of the film shapes that leads to instability as the amplitude of the capillary rim.

SUMMARY

We have examined the effect of gravitational drainage on the stability of a nonvolatile climbing film driven to spread vertically by the application of a constant temperature gradient to the adjacent substrate. The numerical solutions, which are found to be linearly stable to perturbations of all wavenumbers, decrease smoothly and monotonically toward the leading edge. The calculated shape is in excellent agreement with experiments by LL, the only available experiments in the literature on stable climbing films, except for the case

of very low shear stress. Small discrepancies between the theoretical curves and the experimental measurements can easily be accounted for by inspecting the experimental protocol. For example, for smaller values of the shear stress, it is somewhat difficult to achieve a constant temperature gradient throughout the length of the spreading film. This difficulty, along with the usual uncertainty in predicting the absolute film thickness from interferometry, provides enough latitude for bringing into even better agreement numerical and experimental quantities. The linear stability analysis accurately predicts stable and uniform flow, which is borne out by the extensive set of experiments conducted by LL for time periods ranging from 10 to 24 h. We therefore conclude that gravitational drainage effectively eliminates the formation of the capillary rim observed in unstable spreading films. Nonetheless, the film profiles retain significant curvature and structure upon approach to the precursor layer. We suggest that it is not so much the strong curvature of the film profiles but the maximum amplitude of the capillary rim that engenders unstable flow.

Our results show that stable, uniformly spreading films can be produced by the application of a smaller temperature gradient which produces a thicker film subject to gravitational drainage. This stabilizing mechanism provides a favorable alternative to prewetting the surface with a sizable film, which we previously showed would also stabilize films driven by thermocapillary forces. Our analysis suggests that perhaps other counterflow arrangements can be employed to remove the capillary rim and promote stable flow. Though the counterflow produced with a retarding surface or body force will slow the advance of the spreading film, its presence will ultimately produce homogeneous surface coverage, the most important requirement in coating applications.

APPENDIX: NOMENCLATURE

a	small parameter in initial value problem
A_0	dimensionless strength of van der Waals forces
A_{Ham}	Hamaker constant
b	dimensionless precursor film thickness
c	dimensionless traveling wave speed
Ca	capillary number
E	energy
$\dot{E}_n$	dimensionless normalized rate of energy production for term n
$\dot{E}_{\mathrm{tot}}$	dimensionless normalized rate of total energy production
G	dimensionless eigenfunction associated with streamwise component of disturbance flow
g	gravitational constant
h	film thickness
h_0	dimensionless base flow film profile
h_1	dimensionless disturbance function
h_{c}	characteristic film thickness
h_{exp}	experimental film thickness
l	length scale of inner region
L_{h_0}	linear disturbance operator
n	term index
p	pressure
q	dimensionless disturbance wavenumber
T	temperature
t	time
U	height-averaged velocity in streamwise direction
u	local velocity in streamwise direction
U_{c}	characteristic velocity
U_{exp}	experimentally measured velocity
U_{tw}	traveling wave velocity
V	height-averaged velocity in transverse direction
v	local velocity in transverse direction
x	streamwise coordinate
y	transverse coordinate
z	coordinate perpendicular to substrate

Greek Symbols

α	parameter reflecting the ratio of gravitational to thermocapillary liquid flux
β	dimensionless disturbance growth rate
γ	local surface tension
ζ	dimensionless transverse coordinate
η	viscosity
ξ	dimensionless streamwise coordinate
ρ	density
τ	surface shear stress induced by thermal gradient

ACKNOWLEDGMENTS

The authors gratefully acknowledge support from the National Science Foundation through a Graduate Fellowship (D.E.K.), a CAREER Award (S.M.T.), and a Seed Grant distributed through the Princeton Materials Institute. Partial support from the Exxon Education Foundation and the Can Manufacturers Institute was also used for computational purposes.

REFERENCES

1. Will, F. G., *J. Electrochem. Soc.* **110,** 145 (1963).
2. Bascom, W. D., Cottington, R. L., and Singleterry, C. R., *in* ''Advances in Chemistry Series'' (R. F. Gould, Ed.), Vol. 43, p. 355. American Chemical Society, Washington, DC, 1964.
3. Brzoska, J. B., Brochard-Wyart, F., and Rondelez, F., *Europhys. Lett.* **19,** 2 (1992).
4. Cazabat, A. M., Heslot, F., Troian, S. M., and Carles, P., *Nature* **346,** 824 (1990).
5. Carles, P., and Cazabat, A. M., *J. Colloid Interface Sci.* **157,** 196 (1993).
6. Ludviksson, V., and Lightfoot, E. N., *AIChE J.* **17,** 1166 (1971).
7. Kataoka, D. E., and Troian, S. M., *J. Colloid Interface Sci.* **192,** 350 (1997).
8. Kataoka, D. E., and Troian, S. M., *in* ''Dynamics in Small Confining

Systems III'' (J. M. Drake, J. Klafter, and R. Kopelman, Eds.), Vol. 464, p. 307. Materials Research Society, Pittsburgh, PA, 1997.
9. Huppert, H. E., *Nature* **300,** 427 (1982).
10. Troian, S. M., Herbolzheimer, E., Safran, S. A., and Joanny, J. F., *Europhys. Lett.* **10,** 25 (1989).
11. Moriarty, J. A., Schwartz, L. W., and Tuck, E. O., *Phys. Fluids* **3,** 733 (1991).
12. Spaid, M. A., and Homsy, G. M., *Phys. Fluids* **8,** 460 (1996).
13. Friz, V. G., *Z. Angew. Phys.* **19,** 374 (1965).
14. Tanner, L. H., *J. Phys. D* **12,** 1473 (1979).
15. Tuck, E. O., and Schwartz, L. W., *SIAM Rev.* **32,** 453 (1990).
16. Teletzke, G. F., Davis, H. T., and Scriven, L. E., *Chem. Eng. Commun.* **55,** 41 (1987).
17. Smith, B. T., Matrix Eigensystem Routines: EISPACK Guide, 2nd ed., *in* ''Lecture Notes in Computer Science,'' Vol. 6. Springer-Verlag, New York, 1976.
18. Carles, P., Troian, S. M., Cazabat, A. M., and Heslot, F., *J. Phys. Condens. Matter* **2,** SA477 (1990).